High infrared light yield of Erbium-doped fluoride crystals

F. Chiossi[a,*], S. Vasyukov[a], A. F. Borghesani[b], C. Braggio[a], A. Di Lieto[c], M. Tonelli[c], G. Carugno[a]

[a] *Department of Physics and Astronomy, University of Padua and Istituto Nazionale Fisica Nucleare, sez. Padova via F-Marzolo 8, I-35131 Padua, Italy*
[b] *CNISM Unit, Department of Physics and Astronomy, University of Padua and Istituto Nazionale Fisica Nucleare, sez. Padova via F-Marzolo 8, I-35131 Padua, Italy*
[c] *Department of Physics, University of Pisa, Largo B. Pontecorvo 3, I-56127 Pisa, Italy and NEST - Istituto di Nanoscienze - CNR, Piazza S. Silvestro 12, I-56127 Pisa, Italy.*

Abstract

The emission spectrum of Erbium-doped fluoride crystals excited by soft X-rays in the (400-1700) nm wavelength range is investigated between 3.2 K and 300 K. The largest component of the crystals emission is observed in the infrared range, which corresponds to a light yield of several tens of photons/keV. Such a large value is caused by energy transfer processes between the Erbium ions which convert the excitation of a dopant ion at high energies into the emission of multiple infrared photons. The present results show that this mechanism could be exploited to realize scintillators of high light yield.

Keywords: Erbium, cross relaxation, Infrared light yield.

1. Introduction

The well-known rule that sets the maximum light yield (LY) in a scintillator, LY$< 10^6/(2.5 \cdot E_g)$ where E_g is the material band gap [1–4], has been confirmed by a wide range of experimental data. For instance, some Ce- and Eu-doped compounds (e.g. Ce:$LaBr_3$, Eu:SrI_2) showed the highest LY predicted by the formula. Most scintillators have, however, a much lower efficiency as in $(RE_xY_{1-x})_3Al_5O_{12}$ crystals (RE_x=Nd 1.1%, Tm 4.4%, Ho 2.5%), in which few photons/keV LYs in the visible range have been reported. As the investigated wavelength range was extended, a tenfold infrared (IR) emission intensity was observed as compared to the visible component [5, 6]. Presumably, efficient energy transfer is one of the process responsible for such high LY, but it may not be the only one. These results motivate us to further investigate this subject.

Although the VUV $5d$-$4f$ and visible $4f$-$4f$ transitions of trivalent Er ions doped fluoride matrices have been deeply analyzed by using synchrotron radiation, thorough studies of the LY in the visible and near IR range are missing.

In this paper we want to quantify the soft X-ray excitation response of four heavily Er-doped fluoride crystals (Er:$YLiF_4$ 25%, Er:BaY_2F_8 10%, Er:BaY_2F_8 30%, Er:KY_3F_{10} 30%) in an extended wavelength band. High dopant concentrations should strongly enhance cross relaxation, namely the energy transfer process between Er-Er ions. This process efficiently converts the excitation of a high-lying (>3 eV) Er^{3+} ion into the population of several Er^{3+} ions in low lying levels (<1.5 eV). These levels could

*Corresponding author
Email address: federico.chiossi@phd.unipd.it (F. Chiossi)

be also directly excited by the dopant interaction with secondary electrons. For these reasons, IR LYs are expected to be higher than the maximum theoretical value of 30 photons/keV. Investigation of the scintillation dependence on temperature from 300 K down to 3 K is also carried out in order to give a more thorough understanding of the issue.

2. Theoretical background

It is well-known that the effective lifetime of RE-doped crystals levels can be expressed as [7]:

$$\frac{1}{\tau} = \frac{1}{\tau_R} + W^{MP} + W^{AD}$$

where τ_R is the natural radiative lifetime, W^{MP} the multiphonon relaxation rate, and W^{AD} the dopant-dopant energy transfer rate. Only the last two factors are temperature-dependent but their occurrence rate affects the level emission quantum efficiency and the fluorescence intensity.

The presence of thermal phonons may induce the relaxation of the level via phonon emission that increases the natural process rate according to the formula [8]:

$$W^{MP} = C\exp(-\alpha\Delta E)[1-\exp(h\omega/kT)]^{-\Delta E/h\omega}$$

where C and α are host-dependent parameters, ΔE is the energy gap between the level and the next lower one, and $h\omega$ is the effective phonon energy.

According to the Fermi's Golden-Rule, the energy transfer rate can be written as:

$$W^{\mathrm{AD}} = \frac{2\pi}{\hbar}|\left\langle \Psi_f^{\mathrm{A}}\Psi_f^{\mathrm{D}}\right| H_{\mathrm{int}} \left|\Psi_i^{\mathrm{A}}\Psi_i^{\mathrm{D}}\right\rangle|^2 \int S_a^{\mathrm{A}} S_e^{\mathrm{D}}\,\mathrm{d}E$$

in which there is the squared modulus of the matrix element of the electrostatic interaction between the initial (i) and the final (f) states of the donor (D) and acceptor (A) ions. The integral represents the overlap of the emission spectrum of the donor and the absorption spectrum of the acceptor [9]. However, the strict resonance condition is relaxed when the process is assisted by phonons. In particular, a strong temperature dependence is found when the energy mismatch between the donor and the acceptor is bridged by the absorption thermal phonons.

3. Experimental apparatus

The radioluminescence of the four crystals is studied with two different apparatuses, both exciting with $\approx 20-30$ keV X-rays. The first one allows us to measure the LY at room temperature whereas the second one is used to assess the spectral intensity as a function of temperature.

3.1. Crystal growth

The 2 mm-thick crystals used in this work are grown in the crystal growth facility of the Physics Department of the University of Pisa by using the home-made Czochralski furnace specifically designed for the growth of high quality, optically pure fluoride crystals.

The $YLiF_4$ (YLF) crystal structure is I41/a, namely a tetragonal body centered (I) with a screw axis (41) and a glide plane (/a) symmetries. The unit cell contains four molecules. The lattice parameters are $a = 0.5164$ nm and $c = 1.0741$ nm. The doping RE^{3+} ion substitutes the Y^{3+} ion at a site of S_4 point symmetry [10].

The KY_3F_{10} (KYF) crystal has a cubic structure, with a symmetry belonging to the space group $Fm\bar{3}m$. The unit cell contains eight molecules and the lattice parameter is $a = 1.15439$ nm. The doping RE^{3+} ion substitutes the Y^{3+} ion at a site of C_{4v} point symmetry [11].

The BaY_2F_8 (BYF) crystal is monoclinic belonging to the C_2/m space group. The unit cell has three different dimensions and one angle greater than 90°: $a = 0.6983$ nm, $b = 1.0519$ nm and $c = 0.4264$ nm with $\beta = 99.68°$. The doping RE^{3+} ion substitutes the Y^{3+} ion at a site of C_2 point symmetry [12].

All crystals are grown by starting from raw materials of 5N or 6N purity supplied by AC Materials (Orlando, FL, U.S.A.). The starting powders are BaY_2F_8, ErF_3, BaF_2, YF_3, LiF, KY_3F_{10}, KEr_3F_{10}, in appropriate proportions to obtain the expected dopant concentrations. The KY_3F_{10} crystals are grown following the method developed (and recently patented [13]) to obtain very good optical properties.

The growth is carried out at a temperature varying from 850 °C (for YLF) up to 1000 °C (for KYF), in an inert atmosphere of pure (5N) argon. The boules

are oriented along the crystallographic axes by using a X-rays Laue machine. For the BYF crystals also the optical axes are identified before cutting the samples. All the samples are also polished to optical quality, and their spectroscopic quality is checked by recording the absorption spectra with a commercial spectrophotometer (Cary 500) before their use in all experiments.

3.2. Light yield estimation

The experimental apparatus and the relative LY measurement procedure have thoroughly been described in literature [5, 14, 15]. We only recall here the main features. An adjustable and continuous current of 70 keV electrons impinges on a thin Tantalum foil. The low-energy fraction of the produced X-rays is blocked by a thin carbon tape whereas the remaining one is completely absorbed within the crystal owing to its still low energy. The light emission of the crystal is investigated in the 500-900 nm range by a Silicon photodiode (PD) (Hamamatsu mod. S1337-1010BQ) with bandpass filter (FESH900, Thorlabs) and in the 900-1700 nm band by an InGaAs PD (Thorlabs, DET20C) with longpass filter (FELH900, Thorlabs). Their output is then amplified by a charge amplifier.

A mechanical chopper with a rotation frequency of 10 Hz is mounted between the crystal and the PD and the averaged ratio between the charge per pulse of the PD signal and the injected current is measured for several values of injected current. By taking into account the properties of the two PDs and comparing their response with a calibrated crystal (Pr:LuYAG 0.16%) it is possible to quantify the LY in the two bands within an accuracy of 15%. In order to obtain a higher signal-to-noise ratio, the chopper is removed and the emission spectra are acquired using InGaAs and Si CCD-based spectrometers.

3.3. Temperature dependence investigation

The temperature dependence of the fluorescence intensity is investigated by using a two-stage cold head cryogenic system (Oerlikon Leybold Coolpower) coupled with a heater (Lake Shore HTR-25). The second stage allows us to cool the crystal sample at any desired temperature between 300 K and 3.2 K. A silicon diode (DT-670-DI) is used to measure the temperature of the crystal. The X-rays excitation is provided by a X-rays tube (Oxford Jupiter 5000) and can be pulsed at several tens of Hz by a 5 mm thick lead chopper. The crystal scintillation light crosses a BaF_2 optical windows and is coupled to the input of a fiber spectrometer (QE-PRO, OceanOptics) or to the active area of an InSb detector (J10D-M204-R02M-60, EG&G Judson) to probe the (1-5) μm wavelength region. In the first case, the emission spectrum in the (300-1050) nm range is acquired. In the second case, the X-rays excitation is pulsed and the InSb PD output is connected to a lock-in amplifier to improve the signal-to-noise ratio.

The emission spectral intensity and the InSb PD output are recorded for identical excitation intensity as a function of the sample temperature. In particular, the InSb PD is used to analyse the total integrated emission in the (1500-1700) nm range in which its quantum efficiency is constant. The spectrometer and InSb PD therefore provide the temperature dependence of the intensity in each emission band of the Erbium-doped crystals between 300 nm and 1700 nm.

4. Experimental results

4.1. Room temperature emission spectra and light yields

The X-rays luminescence spectra in the 400-1700 nm range recorded at room temperature are shown in Fig. 1. Strong similarities can be seen between all crystals. Actually, all observed transitions can be ascribed to the Er^{3+} emitting manifolds: $^2H_{9/2}$ (410 nm), $^2H_{11/2}$-$^4S_{3/2}$ (550 and 850 nm), $^4F_{9/2}$ (660 nm), $^4I_{11/2}$ (1000 nm), and $^4I_{13/2}$ (1600 nm) bands. The energy levels scheme of Er^{3+} ion in YLF and the above mentioned transitions are shown in Fig. 2.

The relative intensity of the spectral emission in the 500-900 nm and in the 900-1700 nm ranges, obtained by the analysis of the InGaAs and Si PDs signals, has been used to normalize and to merge the spectra acquired by the two spectrometers. This procedure is not only much more accurate than that

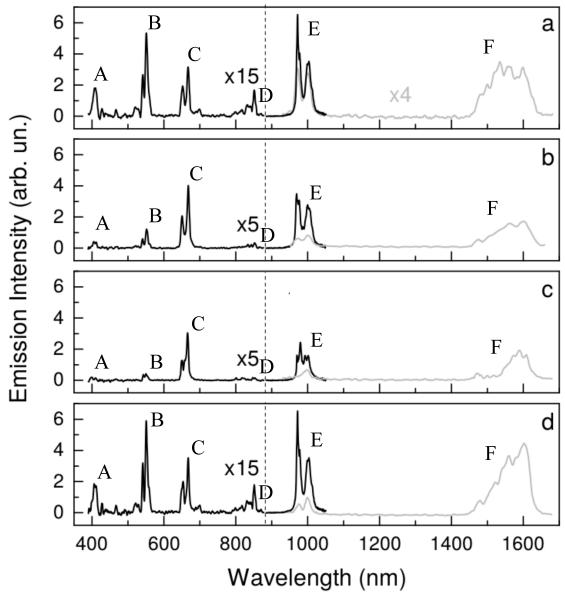

Figure 1: Room temperature, X-rays excited luminescence spectrum of Er:BYF 10% (a) Er:BYF 30% (b) Er:KYF 30% (d), Er:YLF 25% (d) acquired using Silicon (dark line) and InGaAs (light line) CCD-based spectrometers. The labels on the transitions are referring to the labels in Fig. 2.

Table 1: Erbium-doped fluoride crystals LYs at room temperature in the different wavelength ranges.

	LY [photons/keV]	
Crystal	500-900 nm	900-1600 nm
Er:BYF 10%	0.8	51.5
Er:BYF 30%	0.6	40.0
Er:KYF 30%	0.5	30.2
Er:YLF 25%	1.8	133.3

based on the normalization on the common feature at 1000 nm but also provides the absolute LY in the two bands once the response of the calibrated Pr:LuYAG crystal has been measured.

The estimated LYs are reported in Tab. 1. Several tens of IR photons/keV, as high as 133 photons/keV in Er:YLF, are produced by all four fluoride crystals

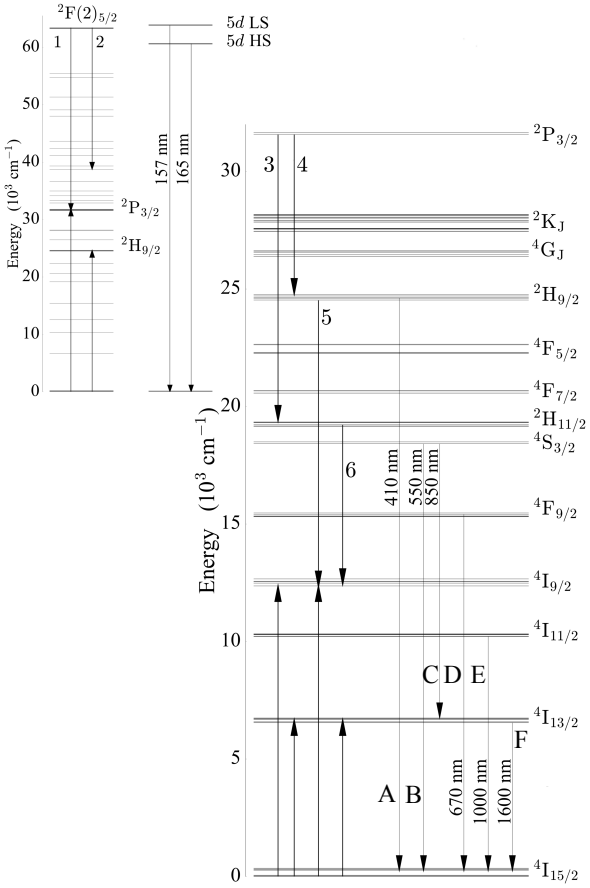

Figure 2: Energy levels scheme of Er:YLF [16, 17]. 4f manifolds in the (0-63 000) cm^{-1} along with the position of the lowest LS and HS 5d levels (left). This scheme is shifted upwards only for the sake of visibility. Detail of the 4f Stark levels up to 34 000 cm^{-1}. Cross relaxation paths and the main radiative transitions are depicted by arrows (right).

against less than 2 photons/keV in the visible range.

4.2. Temperature dependence of the spectral emission intensity

The emission spectra in the 400-1100 nm range have been recorded at several temperaturs. Unfortunately, an intense and minutes-long duration afterglow has been observed at low temperature for all

Table 2: Some cross relaxation pathways in Er:YLF. The process energy difference ΔE (expressed in cm^{-1}) is the smallest one of all the combinations from the lowest Stark level of the initial manifolds and all possible levels of the final manifolds.

#	Initial manifold	Final manifold	ΔE
1	$(^2F(2)_{5/2},^4I_{15/2})$	$\rightarrow (^2P_{3/2},^2P_{3/2})$	< 50
2		$\rightarrow (^4D_{5/2},^2H_{9/2})$	< 30
3	$(^2P_{3/2},^4I_{15/2})$	$\rightarrow (^2H_{11/2},^4I_{9/2})$	49,-3
4		$\rightarrow (^2H_{9/2},^4I_{13/2})$	75
5	$(^2H_{9/2},^4I_{15/2})$	$\rightarrow (^4I_{9/2},^4I_{9/2})$	-197
6	$(^2H_{11/2},^4I_{15/2})$	$\rightarrow (^4I_{9/2},^4I_{13/2})$	-1

crystals. In the case of Er:YLF, it significantly increases below 100 K reaching about 25 % of the luminescence intensity during the irradiation.

We subtract a background spectrum recorded at the end of the X-rays excitation to the one registered during irradiation. In this way, the spectral emission intensity for a given temperature is independent of the cooling/heating cycle. All emission spectra are decomposed on few bands corresponding to different emitting manifolds and the areas under the relative curves are determined. Their temperature dependence is plotted in Fig. 3 for Er:YLF and Er:KYF crystals. The behavior of the Er-doped BYF crystals is very similar to that of Er:YLF crystal and it is not worth to be shown here because we are only interested in singling out the physical process responsible for the observed behavior rather than investigating the differences of the manifestation of this process in different crystals.

The dependence of the 1600 nm luminescence collected by InSb is shown in Fig. 3. As the Lock-In amplifier has been employed, the afterglow component is here negligible.

The four crystals share a rough temperature-LY trend. From room temperature down to 50-90 K the visible band intensity related to $^2H_{11/2}$-$^4S_{3/2}$ (545-565 nm) and $^4F_{9/2}$ (645-675 nm) monotonically increases even by a factor $\gtrsim$10 while the intensity of the $\sim$1000 nm and $\sim$1600 nm emission starting from $^4I_{11/2}$ and $^4I_{13/2}$ manifolds is strongly reduced. As the temperature decreases below 30 K, the scintillation progressively grows brighter in all investigated

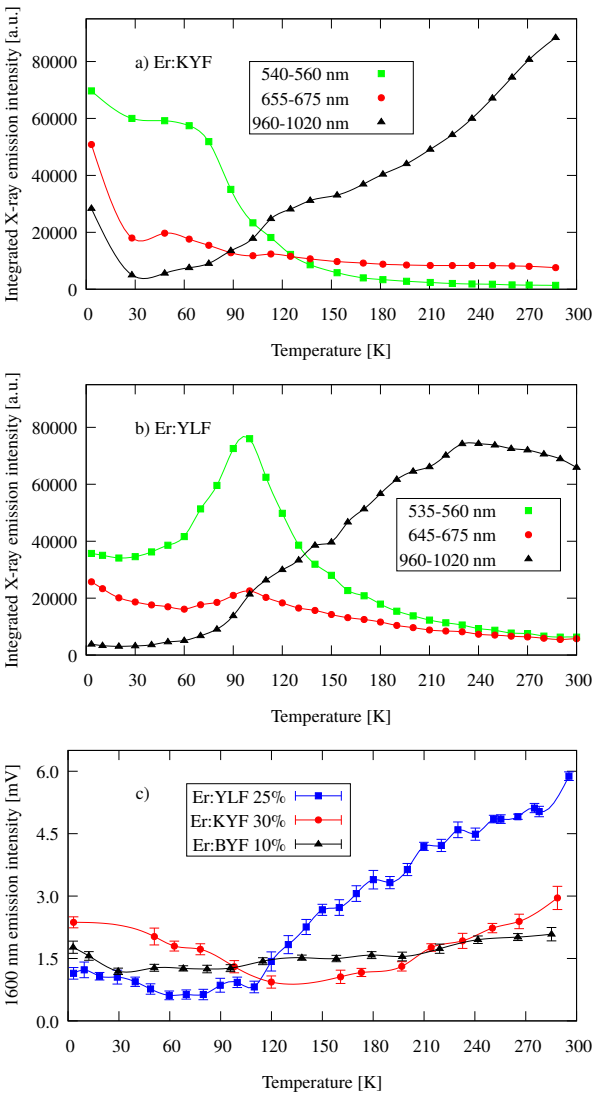

Figure 3: Temperature dependence of the main manifolds emission in visible and near-IR bands for Er:KYF a) and Er:YLF b) crystals and in (1500-1700) nm band c).

wavelength ranges. A plateau at 50 K and an absolute maximum at $\sim$90 K characterize the visible band intensity of the Er:KYF and of the other crystals respectively.

5. Discussion

The results described in this work regarding the LY of heavily Er-doped fluoride crystals can be explained also through the comparison with previous literature. The obtained LY values and their temperature dependence result from several physical mechanisms. Firstly, electron-hole pairs, created by the X-rays absorption, may transfer their energy to the Er^{3+} ions driving them to high energy levels [18]. Secondly, hot electrons and soft X-rays could directly excite the dopant, especially at this concentration. Most importantly, we need to consider the Erbium population/depletion due to multiphonon relaxation and Er-Er ions energy transfer processes. In this case, even the involvement of the $5d$ levels, which cannot be performed with our set up, is considered to explain the high IR LY observed.

VUV and visible luminescence spectroscopy measurements performed with synchrotron radiation in Er-doped fluoride crystals, including YLF, KYF_4 and BYF, led to the following observations:

- The lowest low spin (LS) and high spin (HS) $5d$ levels lie between 60000 and 70000 cm^{-1} and are prone to predominantly relax towards the ground state emitting in the 155-170 nm range with a lifetime of a few hundreds-thousands of nanoseconds [17, 19].

- It has been pointed out that Er ions in YLF can be excited to $5d$ levels only by impact with fast free photoelectrons [20]. The relaxation of self-trapped excitons can only populate the $4f$ levels as their energy is not sufficient to excite the $5d$ levels. The Er^{3+} autoionization and charge transfer between Er^{3+} and F^- ions can also take place even though it is not clear which $4f$ levels get excited.

- $5d$ LS levels are strongly quenched by multiphonon relaxation towards the nearby $5d$ HS levels and $4f$ manifolds as the $^2F(2)_{5/2}$. On the contrary multiphonon relaxation should not play a relevant role for the $5d$ HS level because of the significant separation from the next lower $4f$ levels ($\sim$thousands of cm^{-1}). In addition, the shortening of the $5d$ LS and HS level lifetimes (from 5.6 ns and 5 μs to 3.1 ns and 1.1μs respectively) when the Er concentration is increased to 30%, suggests the occurrence of relevant cross relaxation processes [21].

Because of the rich levels scheme of Er^{3+}, several cross relaxation paths are possible especially for the high energy levels and their occurrence rate is strongly enhanced by increasing the Er ions concentration. Hence, the excitation of $5d$ levels efficiently leads to the population of the lowest $4f$ energy levels. Moreover, the same happens also with the high energy $4f$ manifolds, such as the $^2F(2)_{5/2}$ (63300 cm^{-1}) and $^2P_{3/2}$ (31600 cm^{-1}). Their emission between 390 nm and 520 nm which has been observed in fluorides with 1-2% Erbium doping concentration [17], is missing in our heavily doped crystals at any temperature and, at the same time, the near IR emission is remarkable.

The most promising paths for the $4f$ levels of interest are set out in Tab. 2, partly investigated in Ref. [21, 22]. The $^2F(2)_{5/2}$ relaxation probably results in two ions excited in the $^2P_{3/2}$ manifold or one ion in $^2H_{9/2}$ and one that quickly relaxes non radiatively to $^2P_{3/2}$ levels. Ions in $^2P_{3/2}$ manifolds, in turn, can transfer their energy inducing the population of the $^2H_{11/2}$ or $^2H_{9/2}$ manifolds in which cross relaxation could take place again in favor of the $^4I_{9/2}$ levels population. As the $^4I_{9/2}$ population is quickly depleted by multiphonon relaxation towards the next lower levels, the ultimate result of the subsequent energy transfer processes is the efficient excitation of the $^4I_{11/2}$ and $^4I_{13/2}$ manifolds. In this way, from each Erbium ion excited to high energy levels, up to 5-6 photons in near IR range can be emitted, thereby accomplishing an impressive IR down-conversion. This can reasonably explain the obtained high IR LY values in all tested crystals.

The observed temperature dependence is a further confirmation of the above conclusions. The temperature decrease generally makes energy transfer and multiphonon relaxation less competitive compared to radiative emission and, in turn the down-conversion process is much less efficient. Actually, the $^2H_{11/2}$ and $^4S_{3/2}$ manifolds are thermally coupled. In this

way, the relative population of the former decreases in favor of that of the latter with decreasing temperature according to the Boltzmann distribution. Therefore, even if the cross relaxation involving the $^2H_{11/2}$ manifold is resonant, the effective process rate is reduced by the sample cooling and the $^4S_{3/2}$ photon emission quantum efficiency is enhanced. As concerns the $^2H_{9/2}$ manifold, the cross relaxation process is possible if higher manifold levels are thermally populated or when optical phonons are involved in the process. In fact, the intensity of the $^2H_{9/2}$ and $^4S_{3/2}$ emission at 410 nm, 550 nm and 850 nm increases by a factor > 10 at low temperature, thereby strongly reducing the low-lying manifolds population and emission. The cross relaxation in the case of $^2F(2)_{5/2}$ and $^2P_{3/2}$ manifolds is quasi-resonant, therefore it dominates over the radiative relaxation even at 3 K.

The multiphonon relaxation rate also decreases with the temperature but to a smaller extent than that of the energy transfer processes. For example, the cooling of the samples should reduce the relaxation of the $^4I_{11/2}$ manifold towards the $^4I_{13/2}$ manifold, thereby slightly increasing the emission at $\sim$1 μm. However, a strong reduction is found due to the slowing down of the population of the level via cross relaxation. Energy transfer processes are of no importance for the $^4F_{9/2}$ and the emission increase at 670 nm can be ascribed to a less likely multiphonon relaxation process.

The efficient down-conversion is also enhanced by the re-absorption effect due to the heavily Erbium dopant concentration. A considerable fraction of emitted photons are likely reabsorbed by other Er ions before they leave the crystal, increasing the occurrence of down-conversion processes such as energy transfer. The important role played by the reabsorption effect can be deduced by inspecting the difference between the IR emission spectrum of the Er:BYF doped at 10% and 30%. In fact, the transitions towards the lowest Stark levels are affected by a more intense reabsorption as the level populations follow the Boltzmann distribution and a shift to longer wavelength of the light output spectrum is shown for higher Er^{3+} doping concentration.

Afterglow is due to the release of energy from electron or hole traps that induces an excitation of luminescence centers. In thermoluminescence studies, in which scintillators are irradiated with X-rays at low temperature and the afterglow brightness is measured as function of the increasing temperature, a peak glow is registered for any kind of traps and at a temperature that is related to the trap energy depth [23]. To the best of our knowledge, thermoluminescence investigations on Er-doped fluoride crystals are not reported in literature. However, our results indicates the presence of traps at a corresponding temperature less than 90 K for all the crystals. Hence, the plot in Fig. 3 genuinely reproduces the LY temperature dependence only above 80-110 K, whereas at lower temperature a systematic error is included and only a quality trend can be appreciated.

6. Conclusion

In heavily doped fluoride crystals the scintillation mainly lies in the IR range and its maximum brightness is at room temperature. The LY value measured for Er:YLF is one of the highest ever reported and its non hygroscopic nature makes it even more interesting for applications. Unfortunately, the millisecond-long decay time of the lowest $4f$ levels limits its applicability for scintillating devices. On the other hand, this feature applies to the laser amplified scintillation concept that we have previously proposed for low rate, low energy particle detection [24].

It must be observed that the energy transfer processes may occur even faster than microseconds and that the long decay time is due to the semi-forbidden nature of the rare earth $4f$-$4f$ transitions. Hence, the energy transfer processes responsible for the efficient down-conversion, could be applied for the realization of very bright IR scintillators once the acceptor ion has a fast emission decay time. With the emergence of high count rate, low intrinsic noise, fast single-photon detector in the near- and mid-IR bands [25], a higher performance particle detectors can be devised.

Er-doped crystals have been suggested as possible phosphors for Xe discharge [26]. Through visible photon cascade emission from high energy levels of Er^{3+}, a conversion efficiency as high as 190% may be achieved. However, we have shown that a VUV-near

IR photon conversion with even higher efficiency is possible since energy transfer processes strongly affect also the fast decaying and high $5d$ levels.

Our findings give a deeper insight on the phonon role in the Er levels excitation mechanism and their IR emission intensity. The widely accepted scintillation limit of LY is based on the hypothesis that more than half of the particle energy is converted in phonons within a small volume [3]. As a matter of fact, this temporary high phonon density, much higher than that due to the thermal bath, may accordingly lead to the population of low-lying levels. For instance, only $\sim$15 phonons in fluoride crystals are sufficient to excite the Er^{3+} $^4I_{13/2}$ manifold. In addition, low energy secondary electron could directly interact with Er ions leading the $4f$ population.

However, the temperature dependence of the LYs proves that the energy transfer processes are mainly responsible for the $^4I_{13/2}$ manifold population at room temperature and only a small fraction of the IR scintillation can be ascribed to the mentioned temperature-independent processes.

Acknowlegments

This work is supported by Istituto Nazionale di Fisica Nucleare (INFN) within Demiurgos project. We acknowledge the technical assistance of E. Berto and F. Calaon and the contribution of D. Manicone to the experimental apparatus for temperature dependence measurements. The authors would like to acknowledge I. Grassini for her competence and care in preparing the samples.

Bibliography

[1] A. Lempicki, A.J. Wojtowicz, E. Berman, Nucl. Instrum. Meth. A 333 (1993) 304–311. https://doi.org/10.1016/0168-9002(93)91170-R.

[2] A. Lempicki, A.J. Wojtowicz, J. Lumin. 6061 (1994) 942–947. https://doi.org/10.1016/0022-2313(94)90317-4.

[3] P.A. Rodnyi, P. Dorenbos, C.W.E. van Eijk, Phys. Stat. Sol. b 187 (1995) 15. https://doi.org/10.1002/pssb.2221870102.

[4] P.A. Rodnyi, Physical Processes in Inorganic Scintillators, CRC Press, Boca Raton, FL, 1997.

[5] A. F. Borghesani, C. Braggio, G. Carugno, F. Chiossi, M. Guarise, J. Lumin. 190 (2017) 29–36. https://doi:10.1016/j.jlumin.2017.05.027.

[6] F. Chiossi, A.F. Borghesani, G. Carugno, J. Lumin 203 (2018) 203–207. https://doi.org/10.1016/j.jlumin.2018.06.035.

[7] B. Di Bartolo. "Energy transfer processes in condensed matter". NATO ASI Series, Series B, Physics, vol. 114, 1984.

[8] F. Auzel. Phys. Rev. B 13 (1976) 2809–2817. https://doi.org/10.1103/PhysRevB.13.2809.

[9] N. Yamada, S. Shionoya, T. Kushida, J. Phys. Soc. Jpn, 32 (1972) 1577–1586. https://doi.org/10.1143/JPSJ.32.1577.

[10] R.E. Thoma et al.. J. Phys. Chem. 65 (1961) 1096–1099. https://doi.org/10.1021/j100825a003.

[11] A. Grzechnik, J. Nuss, K. Friese, J.Y. Gesland, and M. Jansen, Z. Kristallogr. 217 (2002) 460. https://doi.org/10.1524/ncrs.2002.217.1.460.

[12] H.P. Jenssen, A. Cassanho. Proc. of SPIE 6100 (2006) 61000W. https://doi.org/10.1117/12.660946.

[13] D. Parisi, S. Veronesi, M. Tonelli. U.S. Patent 20120260846, 2012.

[14] L. Barcellan, E. Berto, G. Carugno, F. Galeazzi, A. F. Borghesani, Rev. Sci. Instrum. 82 (2011) 095103. https://doi:10.1063/1.3636078.

[15] F. Chiossi, K. Brylew, A. F. Borghesani, C. Braggio, C. Carugno, W. Drozdowski, M. Guarise, Nucl. Instrum. Meth. A 855 (2017) 13–15. https://doi:10.1016/j.nima.2017.01.063.

[16] M.A. Couto dos Santos, E. Antic-Fidancev, J.Y. Gesland, J.C. Krupa, M. Lematre-Blaise, P. Porcher, J. Alloy. Compd. 275-277 (1998) 435–441. https://doi.org/10.1016/S0925-8388(98)00363-6.

[17] R.T. Wegh, E.V. Van Loef, G.W. Burdick, A. Meijerink. Mol. Phys. 101 (2003) 1047–1056. https://doi.org/10.1080/0026897021000046906.

[18] A.N. Belsky, J.C. Krupa, DISPLAYS, 19 (1999) 185–196. https://doi.org/10.1016/S0141-9382(98)00049-3.

[19] J. Becker, J.Y. Gesland, N.Yu. Kirikova, J.C. Krupa. V.N. Makhov, M. Runne, M. Queffelec, T.V. Uvarova, G. Zimmerer. J. Lumin. 78 (1998) 91–96. https://doi.org/10.1016/S0022-2313(97)00313-X.

[20] V.N. Makhov, N.M. Khaidukov, N.Yu. Kirikova, M. Kirm, J.C. Krupa, T.V. Ouvarova, G. Zimmerer, J. Lumin. 87-89 (2000) 1005–1007. https://doi.org/10.1016/S0022-2313(99)00507-4.

[21] E. Negodine, Inter- and intraconfigurational luminescence of $LiYF_4$:Er^{3+} under selective VUV excitation, Ph.D. thesis, University of Hamburg (2003).

[22] F. Auzel, Y. Chen, J. Lumin. 65 (1995) 45–56. https://doi.org/10.1016/0022-2313(94)00071-J.

[23] A.J.J Bos, Radiat. Meas. 41 (2007) S45–S56. https://doi:10.1016/j.radmeas.2007.01.003.

[24] A.F. Borghesani, C. Braggio, G. Carugno, F. Chiossi, A. Di Lieto, M. Guarise, G. Ruoso, M. Tonelli, Appl. Phys. Lett. 107 (2015) 193501. https://doi:10.1063/1.4935151.

[25] L. Chen et al.. Opt. Express 26 (2018) 14859–14868. https://doi.org/10.1364/OE.26.014859.

[26] P.S. Peijzel, A. Meijiernink. Chem. Phys. Let. 401 (2005) 241–245. https://doi.org/10.1016/j.cplett.2004.11.049.